Pulmonary Capillary Hemorrhage Induced by Acoustic Radiation Force Impulse Shear Wave Elastography in Ventilated Rats

Douglas L. Miller, PhD ⓘ, *Zhihong Dong, MD, Chunyan Dou, MD, Brandon Patterson, PhD* ⓘ,
Krishnan Raghavendran, MD

Abbreviations

ARFI, acoustic radiation force impulse; CTA, comet tail artifact; DUS, diagnostic ultrasound; IPPV, intermittent positive pressure ventilation; MI, mechanical index; NEEP, negative end-expiratory pressure; PCH, pulmonary capillary hemorrhage; PEEP, positive end-expiratory pressure; PRPA, peak rarefactional pressure amplitude; US, ultrasound

Objectives—Diagnostic ultrasound (DUS) imaging can induce pulmonary capillary hemorrhage (PCH), possibly related to the ultrasonic radiation surface pressure arising from reflection at the lung blood-air interfaces. Acoustic radiation force impulse (ARFI) elastography is a relatively new DUS mode with high-energy "push pulses" used to move tissue and generate shear waves. The objective of this study was to characterize PCH induced by the ARFI elastographic mode for comparison with other previously tested DUS modes.

Methods—Pulmonary capillary hemorrhage induction was examined for ARFI elastographic frames with 5.7-MHz push pulses (Acuson S3000; Siemens Medical Solutions, Mountain View, CA), which had a derated PRPA of 2.6 MPa. Groups of rats with tracheal tube placement had no ventilation (spontaneous breathing), intermittent positive pressure ventilation (IPPV), or IPPV plus 8 cm H_2O of positive end-expiratory pressure (PEEP). Exposure was to 1 or 20 manually triggered image frame acquisitions. The PCH area was measured on the lung surface.

Results—All 20-frame exposure groups, and even the single-frame group, had significant PCH relative to shams. Single-frame exposures produced significantly less PCH ($P = .002$) than 20-frame exposures in rats with a tracheal tube only (spontaneous breathing). The PEEP inhibited the PCH and produced about half of the PCH area induced for IPPV without PEEP ($P = .014$).

Conclusions—The PCH results were comparable with those from a previous study using B-mode or color Doppler exposure for 5 minutes; however, these modes delivered many more pulses for continuous imaging frames, suggesting that the ARFI elastographic frames were individually much more effective.

Key Words—comet tail artifact; diagnostic ultrasound safety; mechanical index; mechanical ventilation; pulmonary diagnostic ultrasound; ultrasound elastography

Diagnostic ultrasound (DUS) imaging of the postnatal mammalian lung can induce pulmonary capillary hemorrhage (PCH).[1] This phenomenon was discovered by Child et al[2] using pulsed ultrasound (US) and has received attention in research designed to quantify US exposure-response trends and to assess the potential safety issue for patients. Authoritative reviews indicate that DUS-induced PCH has been observed in different

mammalian species, as confirmed in different laboratories, and presents a potential risk factor for DUS.[3,4] Direct pulmonary DUS examinations are performed in various clinical settings for diagnosis of pneumonia, pulmonary edema, embolism, pneumothorax, atelectasis, diffuse parenchymal disease, respiratory distress syndrome, and lung cancer.[5–8] The lung may also receive incidental exposure, such as during echocardiography.[4] The use of portable US machines allows DUS examinations to be performed by the physician at the point of care for routine monitoring.[9–11] This widespread use of pulmonary DUS and the apparent safety issue motivates research to define the possible risks of PCH for patients and generate suitable safety guidance.

Our work using DUS systems (early work used single-element laboratory systems) in rats has provided results for US exposure from clinical transducers and imaging.[1] Interestingly the DUS machines causing PCH also show its occurrence in B-mode images as growing comet tail artifacts (CTAs, also known as B-lines).[1] Different modes of US were tested and found to have different PCH exposure-response characteristics.[12] A Vivid 7 Dimension US machine with a 10L linear array transducer (GE Healthcare, Chicago, IL) was used at 6.6 MHz. At the higher power levels, PCH from B-mode or color Angio-mode Doppler imaging produced a band of PCH corresponding to the scan plane, whereas fixed-beam M-mode or pulsed Doppler-mode imaging produced an isolated spot of PCH. Pulse peak rarefactional pressure amplitude (PRPA) thresholds were 1.5 MPa for the B-mode, 1.1 MPa for the Angio Doppler mode, 1.1 MPa for the M-mode, and 0.6 MPa for the pulsed Doppler mode. The pulsed Doppler mode had relatively long pulses (1130 versus 269 nanoseconds for M-mode) and a relatively high exposure duty cycle (7.7×10^{-3} versus 0.27×10^{-3} for M-mode), which may explain its relatively low threshold.

The physical mechanism for PCH induced by pulsed US has not been clearly established.[13] Diagnostic US-induced PCH has thresholds that are well defined for a given set of conditions but vary for different specific situations. Thresholds for PCH do not have a clear frequency dependence,[14] which suggests that a frequency-independent mechanism, such as the ultrasonic radiation pressure on the lung surface, may

be important for induction of PCH.[13] High-intensity focused US can perturb a liquid surface and produce fountains and atomization, which might also play a role in DUS-induced PCH.[15–17] Pulmonary capillary hemorrhage induction depends on physical exposure parameters, including the pulse duration, pulse repetition frequency, and exposure duration, in addition to the PRPA.[4] In addition, DUS-induced PCH depends on physiologic conditions; for example, PCH induction in rats with anesthesia using only ketamine is increased substantially when xylazine is used together with ketamine for anesthesia.[18]

Diagnostic US-induced PCH also was strongly influenced by intermittent positive pressure ventilation (IPPV).[19] In addition to IPPV, which simulates a normal respiration volume and rate, positive end-expiratory pressure (PEEP) was applied. By maintaining positive pressure, PEEP tends to compress the capillaries, reduce transcapillary pressure, and reduce capillary perfusion.[20] Positive end-expiratory pressure is often used clinically at a low value of 4 to 5 cm H_2O to maintain oxygenation and prevent alveolar collapse. Higher PEEP can be used to recruit alveoli and minimize pulmonary edema.[21] Intubated rats received normal positive pressure ventilation (IPPV) with 0 end-expiratory pressure, IPPV plus +4 cm H_2O of PEEP, or IPPV plus –4 cm H_2O of negative end-expiratory pressure (NEEP).[19] An HDI 5000 US machine was used with a CL15-7 compact linear array transducer (Philips Healthcare, Bothell, WA) at 7.6 MHz. The use of NEEP enhanced PCH, and PEEP virtually eliminated PCH compared with normal IPPV. Threshold PRPAs were 1.3 MPa for IPPV, 2.1 MPa for IPPV plus PEEP, and 1.0 MPa for IPPV plus NEEP. The ± 4-cm H_2O variation in pressure was small (eg, atmospheric pressure is ≈ 1000 cm H_2O), but comparable in magnitude with the expected ultrasonic radiation surface pressure. Note that the application of PEEP was a test for the importance of very small pressures on the gas side of the pulmonary blood-air barrier, which oppose the small ultrasonic radiation surface pressure, and not a test for the cavitation mechanism of bioeffects. Ultrasonic cavitation does not appear to be responsible for DUS-induced PCH,[13] and tests of the role of cavitation in bioeffects, for example, in lung[22] or focused US atomization,[23] require much higher static pressures higher than 1 MPa (>10,000 cm H_2O).

Diagnostic US elastography using acoustic radiation force impulses (ARFIs) to probe tissue has been developed to provide information on tissue stiffness, and this new DUS mode presents substantially different US exposure from the other imaging modes noted above. Several different DUS elastographic methods are available,[24,25] and ARFI elastography is used clinically for assessments of breast,[26] liver,[27] and other tissues. For ARFI elastography, relatively long US pulses (often called "push pulses") are used to cause tissue in the US beam to move with displacements that can exceed 10 μm.[28,29] The displacements can be measured by evaluation of tissue echoes or by US measurement of the shear waves generated by the impulsive motion. The shear wave method allows quantitative measurements of shear wave velocity and tissue elasticity estimates.

The use of push pulse methods in DUS elastography might be considered a qualitatively different type of US exposure from conventional DUS, and possible specific bioeffects that could be associated specifically with ARFI elastography have received some consideration. The potential for excessive ultrasonic heating has been of interest because of the long-duration ARFI elastographic pulses.[30–32] In soft tissue, the temperature elevations for single push pulses appear to be a few degrees Celsius, but elevations in bone could be much higher, and bone should be avoided in ARFI elastography. The temperature elevations created by repeated ARFI image frames potentially can build to values that are of concern; therefore, interframe intervals should be sufficient to avoid excessive heat buildup.[32]

Takayama et al[33] reported PCH in a rabbit exposed to ARFI elastography-like pulses from a custom-made transducer. The 2.5-MHz pulses were 10 milliseconds in duration and repeated at 5-second intervals for 150 seconds. The PCH area was visible on the surface and was observed in histologic sections to be 20 to 170 μm below the surface.

The dependence of PCH induced by pulsed US on the pulse duration was investigated by Child et al.[2] For 10-microsecond pulses, increasing the pulse repetition period from 1 to 10 milliseconds had no effect on the PCH threshold in mice, whereas decreasing the pulse duration to 1 microsecond with a 10-millisecond pulse repetition period increased the threshold. A trend of decreasing thresholds for increasing pulse durations from 1.3 to 11.6 microseconds was also found by O'Brien et al.[34] The thresholds also depend on the overall exposure duration for laboratory pulsed[35] and diagnostic scanned US.[36] The pulsed Doppler mode of DUS was substantially more effective than the M-mode, as noted above.

Acoustic radiation force impulse elastography uses scanned, relatively long-duration push pulses, plus repeated shear wave interrogation pulses, and might be expected to have a greater PCH impact than the other modes. This study was undertaken to assess PCH occurrence in rats due to single and multiple ARFI elastographic frames from a clinical US machine. The PCH associated with the push pulses was specifically examined by reducing the output of the other pulses to 5% of the maximum. In addition, IPPV was used with PEEP of 8 cm H_2O for comparison with the previous study of the influence of IPPV plus PEEP. The goals were to characterize DUS-induced PCH from the ARFI elastographic mode for comparison with other previously tested DUS modes and to assess the relative reduction in PCH due to added PEEP.

Materials and Methods

Animal Preparation

All in vivo animal procedures were conducted with the approval and guidance of the Institutional Animal Care and Use Committee of the University of Michigan. Female rats (Sprague Dawley; Charles River, Wilmington, MA) were used for this study, as described previously.[1] Rats were anesthetized by intraperitoneal injection of 91-mg/kg ketamine (Zetamine ketamine hydrochloride injection; MWI, Boise, ID) plus 9-mg/kg intraperitoneal xylazine (XylaMed xylazine injection; MWI), which is the recommended anesthetic for rats. The right thorax was shaved and depilated for US transmission. A tracheostomy was performed, and the trachea was intubated with a plastic tube (2.2-mm outer diameter and 1.3-mm inner diameter) with Luer lock fitting. For US exposure, the rats were mounted on a holding board in the dorsal recumbent position, and the board was mounted vertically in a 38°C degassed water bath. This allowed for accurate US imaging and

exposures of the right lung with US transducers also mounted in the water bath.

The tracheal tube was stabilized on the mounting stand for connection to a ventilator as needed. The rats were able to breathe spontaneously through the tracheostomy tube. For normal IPPV, a rodent ventilator (TOPO dual-mode ventilator; Kent Scientific, Torrington, CT) was connected by a tubing tee. The normal ventilator setting was a respiration rate of 75 breaths per minute with 25% positive inspiration at 15 cm H_2O during the ventilation cycle, as recommended for rats in the operator's manual. To generate 8 cm H_2O of PEEP, a bottle of water containing 8 cm of water was attached to the expiration port of the ventilator. The ventilation pressure and PEEP were confirmed with a low-pressure gauge (± 5 PSI Traceable; Fisher Scientific Co, Houston, TX).

Ultrasound

An Acuson S3000 US machine with a 9L4 Multi-D matrix transducer (Siemens Medial Solutions, Mountain View, CA, USA) was used in the Virtual Touch IQ mode. The transducer was mounted in the water bath and B-mode imaging at 5% power was used to aim through an intercostal space at the right cranial or medial lobe of the rat lung. Scanning used a 3-cm image depth, 3.66-cm image width, 2-cm focal depth, and the MultiHz 9-MHz setting. For Virtual Touch IQ elastography, the elastographic image box was expanded to the maximum size of 2.55 cm deep ×

3.66 cm wide, starting at a 0.2-cm depth. For exposure, the lung surface image was adjusted to place the closest point at a 1.4-cm image depth. The power setting of 5%, which gave an on-screen mechanical index (MI) of 0.3 (below the PCH threshold for B-mode), was retained for exposure so that only the effects associated with the ARFI elastographic push pulses would occur. The output for the ARFI push pulses could not be reduced, which prevented a determination of an exposure threshold for PCH using this mode. The system enforced a cooldown interval of 5 seconds after an ARFI frame during which a frame update could not be triggered. The exposure consisted of 1 or 20 manually initiated frames at intervals of about 15 to 18 seconds (including the cooling period, reset time, and the time needed to save images). The elastographic image was color mapped for shear wave velocity and had a scale of 0.5 to 6.5 m/s.

The US pulse parameters were measured in the water bath by a calibrated hydrophone with a 0.2-mm sensitive spot (HGL-0200; Onda Corp, Sunnyvale, CA). The hydrophone was visible in the image and was placed at the 1.4-cm depth corresponding to the surface of the lung during exposures and moved along the scan plane to find the position of the maximum PRPA of the ARFI pulses. Pulse waveforms were digitized on an oscilloscope and transferred to a computer for determination of pulse characterization parameters. The ARFI elastography involves 2 types of pulses, push pulses and sets of B-mode–like pulses,

Figure 1. Plots of the ARFI elastographic waveforms from a hydrophone, which were digitized on an oscilloscope and derated for attenuation. The hydrophone measures the ultrasonic pressure at its position in the scan plane as a function of time set by a trigger point (0 time in these plots). The waveforms are more complex than a simple B-mode scan and include B-mode image pulses, ARFI image push pulses, and shear wave interrogation pulses. The maximal push pulse is indicated by the arrow in **A**, which shows the sequence of 4 ARFI image scans (see "Materials and Methods"), and is displayed in **B** at a higher temporal resolution to show the pair of long pulses that make up the push pulse.
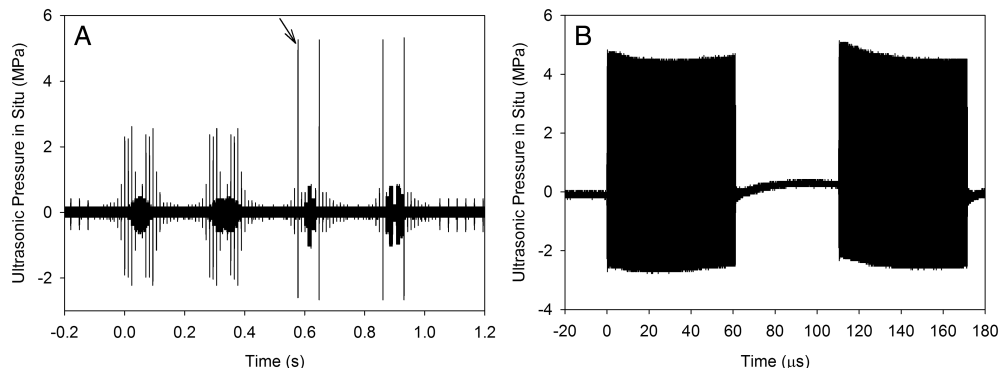
which interrogate shear wave motion and provide the background grayscale image. An ARFI elastographic pulse sequence is shown in Figure 1A and was about 1.1 seconds in duration. This complex sequence shows 92 ARFI push pulses spaced about 11.8 milliseconds apart, which have different amplitudes due to the beam scanning or focus depth differences. The 4 equal maximal push pulses were recorded when the scanned beam was aimed directly at the hydrophone. The pulses were grouped into 4 similar sets of scans spaced 286 milliseconds apart. The maximal push

pulses of interest for this study were pairs of 5.7-MHz continuous wave bursts 61 microseconds in duration and spaced 49 microseconds apart, as shown in Figure 1B. The –6-dB beam width of the push pulses was 3 mm. The water values of US pressure amplitudes were derated by 1.2 dB/cm/MHz, which was equal to –3.4 dB for the chest wall thickness of about 0.5 cm, to obtain in situ values.[14] The derated push pulse peak compressional pressure amplitude, PRPA, and mean pressure amplitude were 5.0, 2.6, and 3.8 MPa, respectively. The derated PRPA was used to

Figure 2. B-mode images were acquired just before (top left) and 5 minutes after (top right) 20 ARFI elastographic frames for the exposure tests without IPPV (tracheal tube but spontaneous breathing). The after-exposure image shows CTAs extending across most of the bright-line surface image seen before exposure. The resulting PCH areas on the right lung are shown in the bottom image (scale bar, 5 mm). The position of the lung in the sample dish reveals PCH areas positioned on the cranial (top right) medial (bottom) and caudal (top left) lobes.
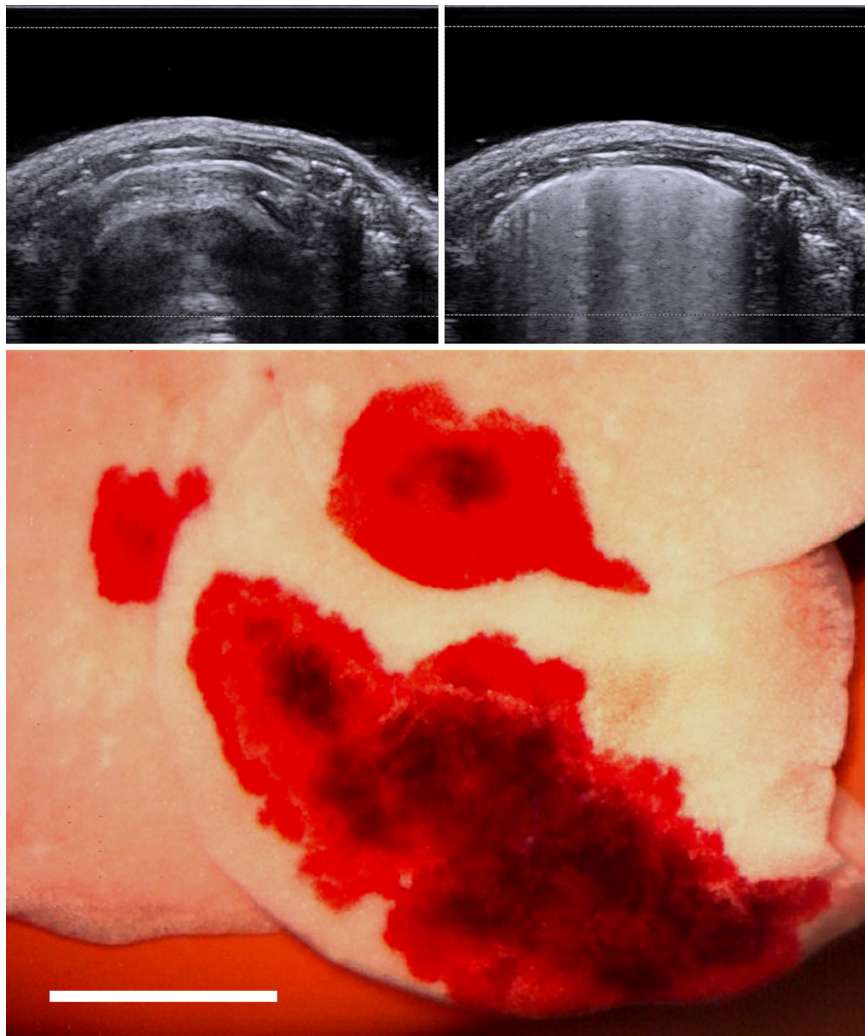
calculate the in situ MI as the PRPA divided by the square root of 5.7 MHz, which was equal to 1.1. The derated pulse waveform was used to calculate the spatial-peak pulse-average intensity, which was 338 W/cm^2. In addition, the ultrasonic radiation surface pressure was calculated from the derated spatial-peak pulse-average intensity, as described by Miller,[13] and was 45 cm H$_2$O during the maximal push pulses.

Measured End Points

The rats weighed an average of 247 (SD, 14) g. The heart rate and peripheral capillary oxygen saturation were measured with a pulse oximeter probe (SurgiVet V3395 TPR; Smiths Medical, Inc, St Paul, MN) on a front paw before the scanning procedure and were 264 (SD, 36) beats per minute and 76.4% (SD, 8.0%), respectively. Pulmonary capillary hemorrhage—related end points included the percentage of the bright-line image of the lung surface, which was involved with CTAs 5 minutes after exposure. The rat was then euthanized; the trachea was tied off; and the lungs were removed. The right lobes, which were the target of the imaging, were then examined and photographed with a stereomicroscope (S6D, Leica Microsystems,

Figure 3. B-mode images were acquired just before (top left) and 5 minutes after (top right) a single ARFI elastographic frame with the tracheal tube only, presented as in Figure 2. The after-exposure image shows a few small CTAs projecting downward from the center-right region of the lung surface image. The PCH areas consist of numerous small spots on the medial lobe (scale bar, 5 mm).
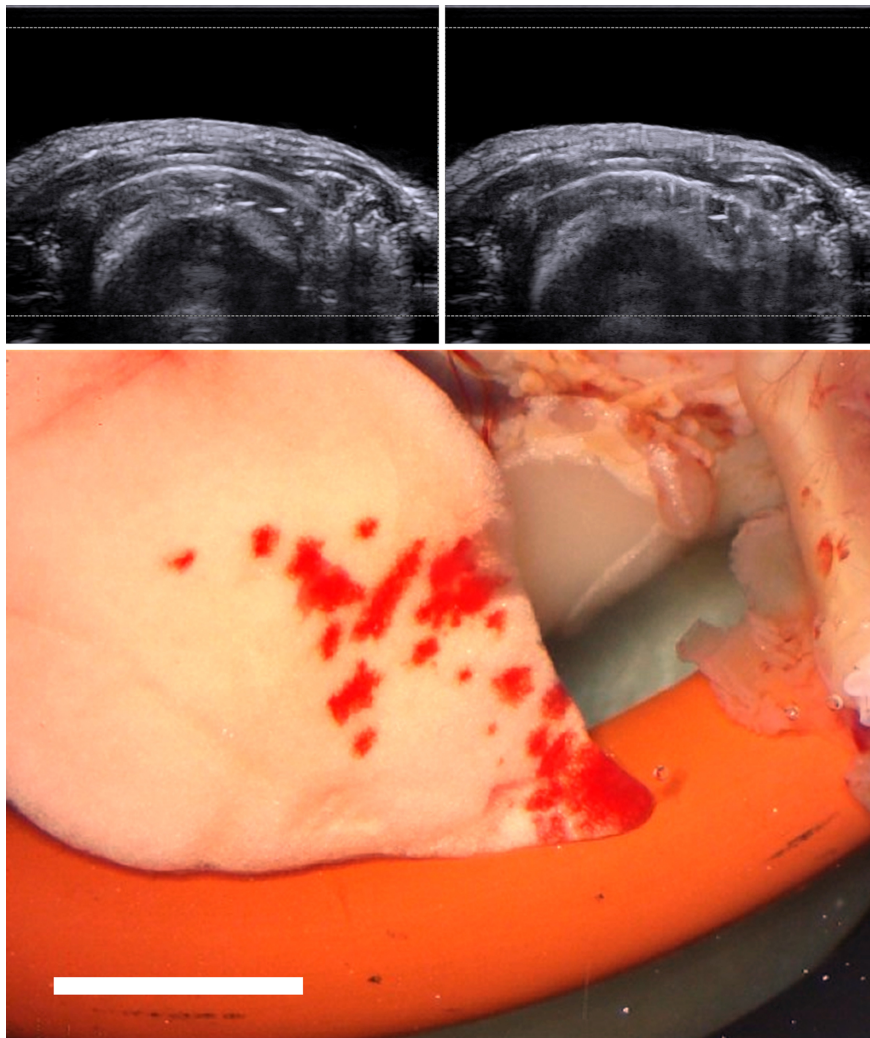
Inc, Buffalo Grove, IL). Digital photographs (Moticam 580; Motic, Richmond, British Columbia, Canada) of the lungs were used to measure the approximate area of the region of PCH on the lung surface by a manual outline of the region, using image analysis with Motic Image Plus 2.0 ML software. The lungs were then fixed in neutral buffered formalin and used to measure the depth of the larger PCH regions to obtain estimates of the PCH volume. Depths were measured in 2-mm intervals by slicing 2-mm-thick sections (the smallest thickness reproducibly attainable by hand sectioning) and

measuring under the stereomicroscope. The mean depth of a PCH volume was then multiplied by the PCH area measured in fresh tissue, as described previously.[36]

Experimental Plan and Statistics

The ARFI push pulses had a fixed output and were triggered by the "update" key on the machine, which triggered generation of a new elastographic image frame. Tracheal tubes were used with spontaneous breathing (no IPPV) in 2 groups of 6 rats. One of these groups was tested with single-frame exposure,

Figure 4. B-mode images were acquired just before (top left) and 5 minutes after (top right) 20 ARFI elastographic frames with IPPV, presented as in Figure 2. The after-exposure image shows CTAs spread across the lung surface image. Substantial PCH areas were produced on the medial lobe (bottom; scale bar, 5 mm), and other PCH areas were found on the cranial and caudal lobes.
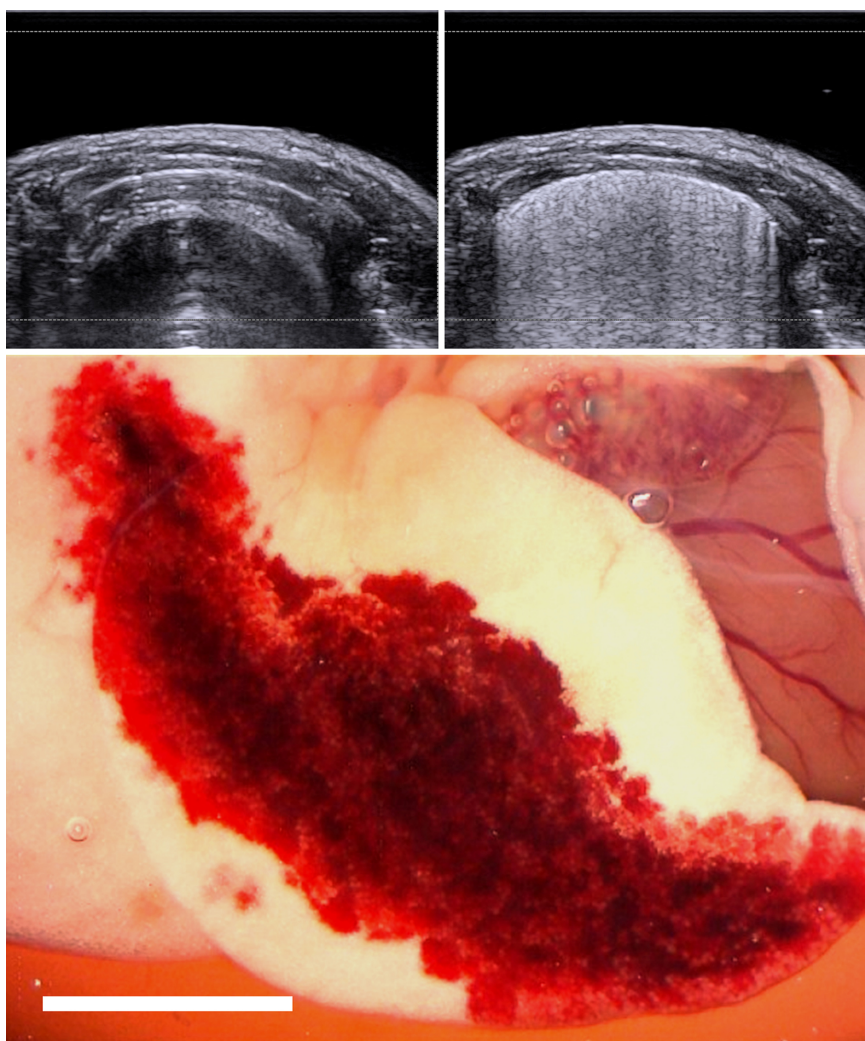
and the other group was tested with 20 frames of exposure, which took about 5 to 6 minutes to complete. One group of 6 rats had IPPV with 20 frames of exposure; IPPV plus 8 cm H_2O of PEEP was used for 6 rats with sham exposure (aim only) and 7 rats with 20 frames of exposure. Statistical significance of the results was determined by a simple t test of the means for exposed versus shams with significance assumed at $P < .05$. Alternatively, results compared as the proportion of rats in a group with PCH occurrence by the Z test with Yates correction (ie, occurrence in 5 of 6 rats was significant) gave the same significance determinations.

Results

The B-mode images of an intubated rat without IPPV saved before and after 20 frames of ARFI elastographic exposure are shown in Figure 2 together with a photograph of the injured lung. The CTAs fill the exposed lung surface image. The lung photograph has all 3 right lung lobes in view, each of which has a PCH area. The PCH areas all occurred in the scan plane in vivo, but the lobes have moved relative to each other after removal. A similar presentation in Figure 3 shows numerous PCH spots on the medial lobe produced by a single frame of ARFI elastography. For this single-frame exposure, the CTAs in the B-mode image taken after exposure are visible as several small artifacts.

Results for a rat with IPPV and 20 frames of ARFI elastography are shown in Figure 4. This lung had a large PCH impact similar to that without IPPV (Figure 2), and the after-exposure B-mode image shows CTAs across the entire lung surface image. The ARFI image of the shear wave velocity did not show any clearly evident changes between the first and last frames, as shown in Figure 5, corresponding to the before and after B-mode images in Figure 4. For this rat, the B-mode images for each of the 20 ARFI frames presented in Figure 6 showed a progressive appearance of CTAs.

When PEEP was applied with IPPV, the PCH effect was often substantial but not as extensive as that found without PEEP, as shown in Figure 7. The B-mode image shows a limited width of CTAs, and the lung photograph has a single large PCH area within part of the scan plane region of the medial

lobe. A noteworthy feature of this lesion was that, although much of the lung appeared to be unaffected, the PCH in the affected area penetrated completely through the lobe, as for the exposures without PEEP.

The measured end-point results are presented in Table 1. The widths of CTAs, which closely tracked the width of PCH on the lungs, were measured as a percentage of the width (which averaged 21.1 ± 2.2 mm) of the bright-line surface image. The percentage of the surface image showing CTAs was essentially 100% for the 20-frame tube-only and IPPV conditions but reduced to 56% ($P = .001$ relative to sham) for IPPV

Figure 5. Elastographic maps acquired at the first (top) and last (bottom) ARFI elastographic frames, which were obtained during the same exposures as the results in Figure 4. There was no apparent change in the elastographic maps due to the exposure. The color map scale included shear wave velocities of 0.5 m/s (blue) to 6.5 m/s (red), with some yellow-to-red areas corresponding to the posterior position of rib and spine structures.
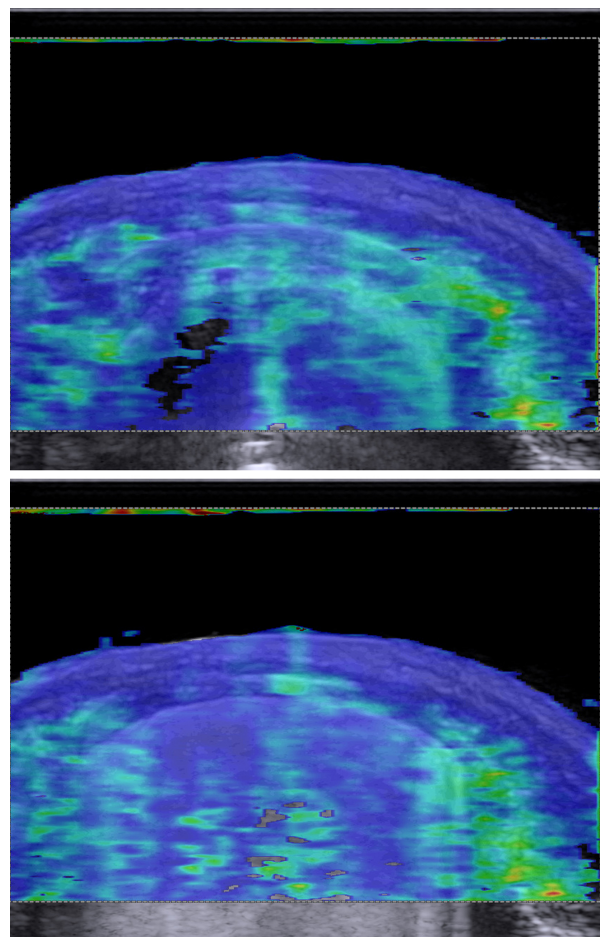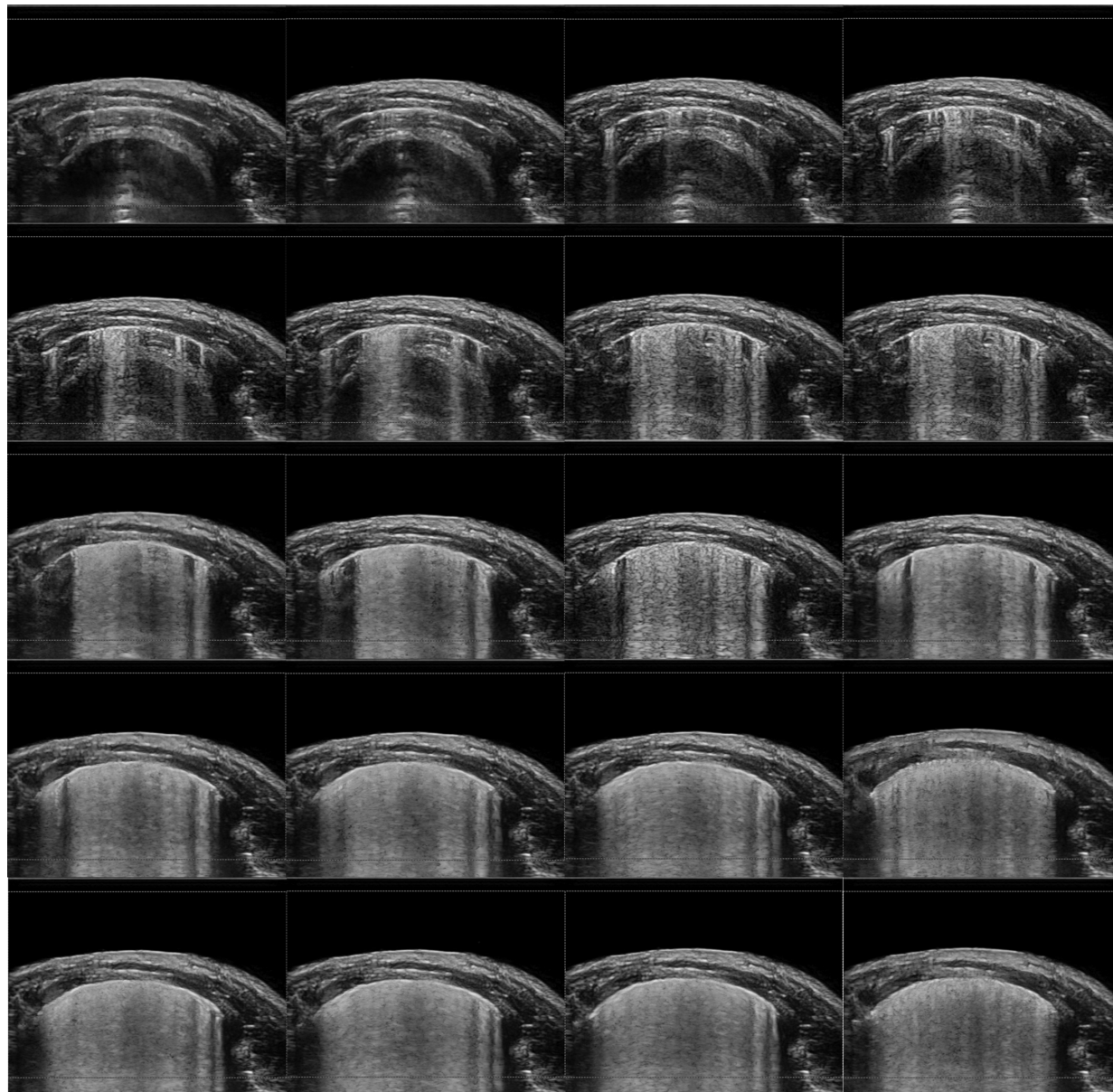
Figure 6. B-mode images acquired for each of the 20 ARFI elastographic frames presented in in rows (ie, frames 1–4 in the top row, etc) The images show the progressive accumulation of CTAs across the bright-line lung surface image between the pre- and post-exposure B-mode images shown in Figure 4.

plus PEEP. The CTAs were only 6% (not significantly different from sham) for the tube-only group exposed to a single elastographic frame. Figure 8 compares the PCH area determined for each test group. The exposed groups, including the single-frame exposure, had statistically significant PCH areas relative to shams. The tube-only and IPPV groups with 20-frame exposure were not significantly different. The single-frame exposure gave a significantly lesser effect than the 20-frame exposure with the tube only ($P = .015$). The use of 8 cm H_2O of PEEP reduced the PCH to about half of the result for the IPPV group ($P < .001$).

Figure 7. B-mode images were acquired just before (top left) and 5 minutes after (top right) 20 ARFI elastographic frames with IPPV plus PEEP, presented as in Figure 2. The after-exposure image shows CTAs spread across about half of the lung surface image. Substantial PCH areas were produced on the medial lobe (bottom; scale bar, 5 mm), and another PCH area was found on the cranial lobe.
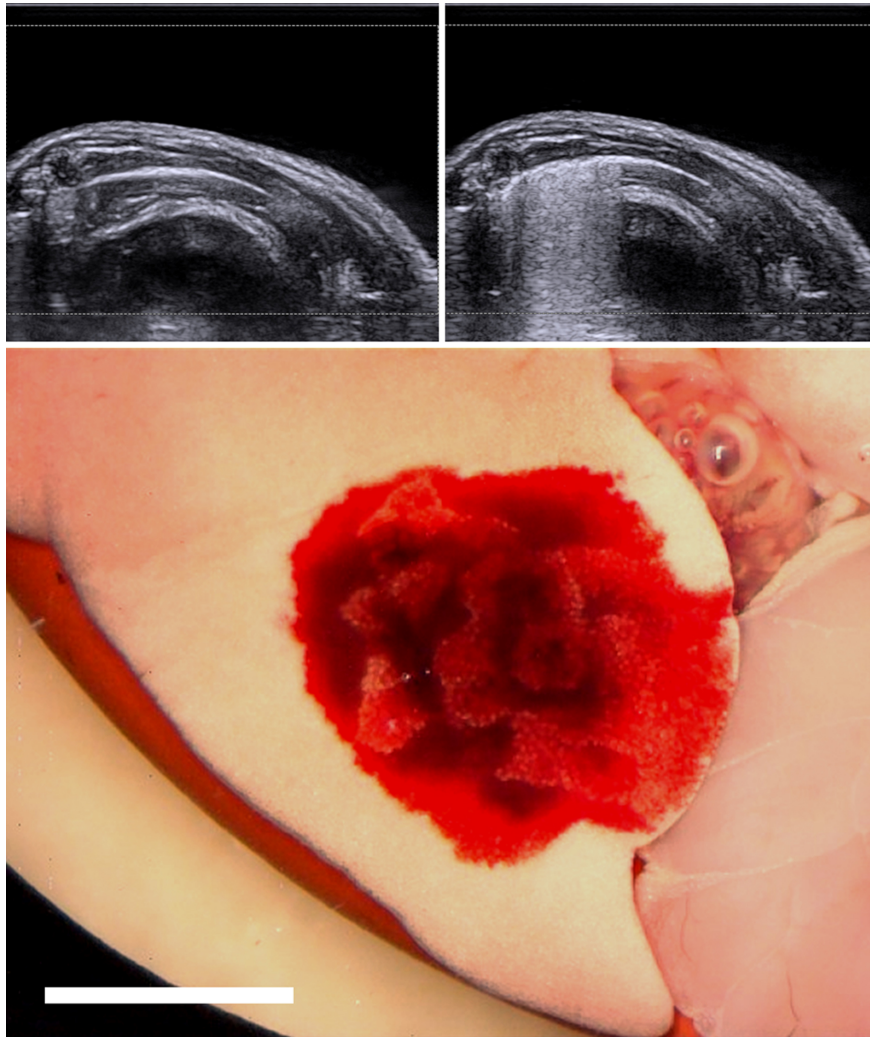
The PCH depth measurements in fixed tissue were partly determined by the thickness of the lobes because many PCH volumes passed entirely through the lobe. The mean depths noted were 1.1 ± 0.6 mm in the cranial lobe, 3.7 ± 0.7 mm in the medial lobe, and 1.5 ± 0.6 mm in the caudal lobe. The mean total PCH volumes in all 3 lobes are listed in Table 1. The PCH volume for IPPV plus PEEP was significantly less than that for the tube-only condition ($P = .017$) and the IPPV condition ($P = .031$).

Discussion

Acoustic radiation force impulse elastography is a relatively new DUS mode with exposure pulse sequences that are distinctly different from other DUS modes. This mode was tested to specifically assess PCH from the 5.7-MHz push pulses, which consisted of two 62-microsecond pulses 49 microseconds apart (Figure 1B), repeated at an 11.8-millisecond interval with a derated PRPA of 2.6 MPa. The PCH produced

by 20 ARFI elastographic frames repeated manually at intervals of about 18 seconds was substantial, filling the scan plane with PCH areas of 36.9 and 34.4 mm^2 for the tube-only and IPPV modes, respectively. Unfortunately, the output was fixed, so that exposure response thresholds could not be determined for this DUS mode. This maximal PCH impact was about the same as for maximal application of other DUS modes. For example, 6.6-MHz B-mode and Angio pulsed Doppler imaging modes were previously tested and had pulse durations of 268 and 319 nanoseconds with 60 and 17.5 frames per second, respectively.[12] These B and Angio Doppler modes produced maximal PCH areas of 45 and 55 mm^2 for derated PRPAs of 3.3 and 2.7 MPa. For 5-minute exposures, however, these modes delivered many more frames (18,000 for B-mode and 5250 for Angio Doppler mode), suggesting that the ARFI elastographic frames were individually much more effective. Indeed, exposure from a single ARFI elastographic frame produced a clear and statistically significant PCH result.

Ventilation with PEEP was used to determine whether the PCH would be greatly inhibited, as it was for B-mode imaging.[19] The PCH was inhibited, but the PCH area observed was still about half that of IPPV without PEEP. The occurrence was variable and was substantial in some rats (Figure 7). For B-mode US, the PCH was essentially eliminated by only 4 cm H_2O, again suggesting that the ARFI push pulses were more effective than the B-mode pulses. Regarding the US radiation surface pressure mechanism, the maximum ultrasonic radiation surface pressure was 22.7 cm H_2O in the previous study for a spatial-peak pulse-average intensity of 168 W/cm^2 compared to 45 cm H_2O for 338 W/cm^2 in this study. A PEEP of 8 cm H_2O was used in this study compared to 4 cm

H_2O in the B-mode study[19] because of the expected higher ultrasonic radiation surface pressure for ARFI elastography. Given the different pulse durations and frame rates, the exact implications for this hypothetical PCH mechanism are not clear.

A better understanding of the pulmonary bioeffects potential of DUS elastography is needed for clinical safety assessments. An investigation of PCH induction by an Aixplorer elastographic machine (SuperSonic Imagine, Aix-en-Provence, France), which incorporates a different push pulse strategy with 1 frame per second and output power variation suitable for exposure-response experiments, should establish the threshold for induction of PCH by push pulses designed to generate shear waves. The diagnostic

Figure 8. Results for the PCH areas for the 5 different conditions listed in Table 1. All exposure conditions were significantly greater than the sham condition, for which no PCH was seen. For the tracheal tube only with spontaneous breathing (Tube), the result for a single frame was significantly less than the result for 20 frames (P = .015). The addition of PEEP to IPPV significantly reduced the PCH (P < .001).
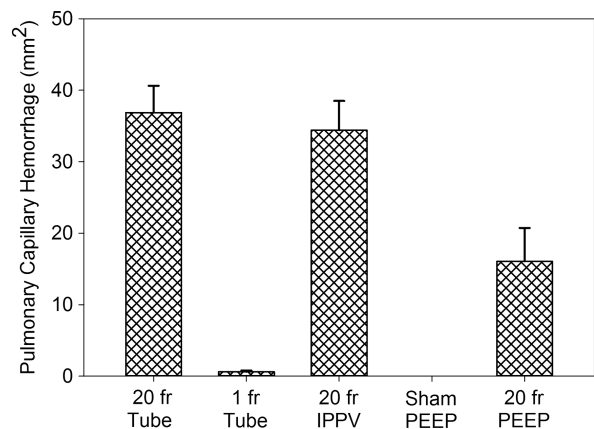
Table 1. Pulmonary Capillary Hemorrhage Results for DUS Scanning in the ARFI Virtual Touch IQ Elastographic Mode

Condition	n	Exposure Frames	CTAs, %	PCH Proportion	Area, mm^2	P	Volume, μL
Tube only	6	20	97 ± 5	6/6	36.9 ± 9.2	.002	97.3 ± 44.9
Tube only	6	1	6 ± 5	5/6	0.61 ± 4.5	.015	NA
IPPV	6	20	90 ± 19	6/6	34.4 ± 10.0	.002	80.6 ± 31.1
IPPV + PEEP	6	0	0	0/6	0	NA	NA
IPPV + PEEP	7	20	56 ± 31	7/7	13.1 ± 12.3	.001	35.3 ± 34.2

Data are presented as mean ± SD where applicable. The single frame with the tube only (spontaneous breathing) was significantly less than the 20-frame exposures (P = .002), and IPPV plus PEEP was significantly less than IPPV (P = .014). The volume of PCH was estimated for the higher-impact conditions. NA indicates not applicable.

value of DUS elastography may be enhanced by conditionally increasing pulse amplitudes, and the use of MI values of up to 4 has been suggested for this purpose.[37] The higher pulse amplitude would represent greatly increased exposure relative to this study, with an in situ MI of 1.1. Further research is needed to clarify PCH mechanisms. High-intensity focused US directed upward at a liquid surface can produce fountains and atomization, phenomena that can be responsible for tissue fragmentation and might be involved in PCH.[15–17,23] We have found that the present push pulses (limited to a DUS MI <1.9) can produce fountains and atomization at a water- or blood-air interface.[38] A study of the fountain and atomization phenomena with different DUS modes should help gauge their importance in PCH. This information will establish whether DUS elastography represents a qualitatively different exposure regimen for PCH risk from other DUS modes.

References

1. Miller DL. Induction of pulmonary hemorrhage in rats during diagnostic ultrasound. *Ultrasound Med Biol* 2012; 38:1476–1482.

2. Child SZ, Hartman CL, Schery LA, Carstensen EL. Lung damage from exposure to pulsed ultrasound. *Ultrasound Med Biol* 1990; 16: 817–825.

3. American Institute of Ultrasound in Medicine. Section 4: bioeffects in tissues with gas bodies. *J Ultrasound Med* 2000; 19:97–108, 154–168.

4. Church CC, Carstensen EL, Nyborg WL, Carson PL, Frizzell LA, Bailey MR. The risk of exposure to diagnostic ultrasound in postnatal subjects: nonthermal mechanisms. *J Ultrasound Med* 2008; 27:565–592.

5. Sartori S, Tombesi P. Emerging roles for transthoracic ultrasonography in pleuropulmonary pathology. *World J Radiol* 2010; 2:83–90.

6. Volpicelli G. Lung sonography. *J Ultrasound Med* 2013; 32:165–171.

7. Lichtenstein D. Lung ultrasound in the critically ill. *Curr Opin Crit Care* 2014; 20:315–322.

8. Dietrich CF, Goudie A, Chiorean L, et al. Point of care ultrasound: a WFUMB position paper. *Ultrasound Med Biol* 2017; 43:49–58.

9. Ahmad S, Eisen LA. Lung ultrasound: the basics. In: Lumb P, Karakitsos D (eds). *Critical Care Ultrasound*. Philadelphia, PA: Elsevier; 2015:105–137.

10. Irwin Z, Cook JO. Advances in point-of-care thoracic ultrasound. *Emerg Med Clin North Am* 2016; 34:151–157.

11. Sekiguchi H. Tools of the trade: point-of-care ultrasonography as a stethoscope. *Semin Respir Crit Care Med* 2016; 37:68–87.

12. Miller DL, Dong Z, Dou C, Raghavendran K. Pulmonary capillary hemorrhage induced by different imaging modes of diagnostic ultrasound. *Ultrasound Med Biol* 2018; 44:1012–1021.

13. Miller DL. Mechanisms for induction of pulmonary capillary hemorrhage by diagnostic ultrasound: review and consideration of acoustical radiation surface pressure. *Ultrasound Med Biol* 2016; 42: 2743–2757.

14. Miller DL, Dou C, Raghavendran K. The dependence of thresholds for pulmonary capillary hemorrhage on diagnostic ultrasound frequency. *Ultrasound Med Biol* 2015; 41:1640–1650.

15. Tjan KK, Phillips WRC. On the impulsive generation of drops at the interface of two inviscid fluids. *Proc R Soc A* 2008; 464:1125–1140.

16. Tjan KK, Phillips WRC. On impulsively generated inviscid axisymmetric surface jets, waves and drops. *J Fluid Mech* 2007; 576:377–403.

17. Simon JC, Sapozhnikov OA, Khokhlova VA, Wang YN, Crum LA, Bailey MR. Ultrasonic atomization of tissue and its role in tissue fractionation by high intensity focused ultrasound. *Phys Med Biol* 2012; 57:8061–8078.

18. Miller DL, Dou C, Raghavendran K. Anesthetic techniques influence the induction of pulmonary capillary hemorrhage during diagnostic ultrasound in rats. *J Ultrasound Med* 2015; 34:289–297.

19. Miller DL, Dong Z, Dou C, Raghavendran K. Pulmonary capillary hemorrhage induced by diagnostic ultrasound in ventilated rats. *Ultrasound Med Biol* 2018; 44:1810–1817.

20. Nieman GF, Paskanik AM, Bredenberg CE. Effect of positive end-expiratory pressure on alveolar capillary perfusion. *J Thorac Cardiovasc Surg* 1988; 95:712–716.

21. Wiesen J, Ornstein M, Tonelli AR, Menon V, Ashton RW. State of the evidence: mechanical ventilation with PEEP in patients with cardiogenic shock. *Heart* 2013; 99:1812–1817.

22. O'Brien WD Jr, Frizzell LA, Weigel RM, Zachary JF. Ultrasound-induced lung hemorrhage is not caused by inertial cavitation. *J Acoust Soc Am* 2000; 108:1290–1297.

23. Simon JC, Sapozhnikov OA, Wang YN, Khokhlova VA, Crum LA, Bailey MR. Investigation into the mechanisms of tissue atomization by high-intensity focused ultrasound. *Ultrasound Med Biol* 2015; 41:1372–1385.

24. Doherty JR, Trahey GE, Nightingale KR, Palmeri ML. Acoustic radiation force elasticity imaging in diagnostic ultrasound. *IEEE Trans Ultrason Ferroelectr Freq Control* 2013; 60:685–701.

25. Shiina T, Nightingale KR, Palmeri ML, et al. WFUMB guidelines and recommendations for clinical use of ultrasound elastography, part 1: basic principles and terminology. *Ultrasound Med Biol* 2015; 41:1126–1147.

26. Barr RG, Nakashima K, Amy D, et al. WFUMB guidelines and recommendations for clinical use of ultrasound elastography, part 2: breast. *Ultrasound Med Biol* 2015; 41:1148–1160.

27. Ferraioli G, Filice C, Castera L, et al. WFUMB guidelines and recommendations for clinical use of ultrasound elastography, part 3: liver. *Ultrasound Med Biol* 2015; 41:1161–1179.

28. Palmeri ML, Sharma AC, Bouchard RR, Nightingale RW, Nightingale KR. A finite-element method model of soft tissue response to impulsive acoustic radiation force. *IEEE Trans Ultrason Ferroelectr Freq Control* 2005; 52:1699–1712.

29. Palmeri ML, Nightingale KR. Acoustic radiation force–based elasticity imaging methods. *Interface Focus* 2011; 1:553–564.

30. Palmeri ML, Nightingale KR. On the thermal effects associated with radiation force imaging of soft tissue. *IEEE Trans Ultrason Ferroelectr Freq Control* 2004; 51:551–565.

31. Palmeri ML, Frinkley KD, Nightingale KR. Experimental studies of the thermal effects associated with radiation force imaging of soft tissue. *Ultrason Imaging* 2004; 26:100–114.

32. Liu Y, Herman BA, Soneson JE, Harris GR. Thermal safety simulations of transient temperature rise during acoustic radiation force-based ultrasound elastography. *Ultrasound Med Biol* 2014; 40:1001–1014.

33. Takayama N, Ishiguro Y, Taniguchi N, et al. The effect of ultrasound with acoustic radiation force on rabbit lung tissue: a preliminary study. *J Med Ultrason* 2016; 43:481–485.

34. O'Brien WD, Simpson DG, Frizzell LA, Zachary JF. Threshold estimates and superthreshold behavior of ultrasound-induced lung hemorrhage in adult rats: role of pulse duration. *Ultrasound Med Biol* 2003; 29:1625–1634.

35. Miller DL, Dou C, Raghavendran K. Pulmonary capillary hemorrhage induced by fixed-beam pulsed ultrasound. *Ultrasound Med Biol* 2015; 41:2212–2219.

36. Miller DL, Dong Z, Dou C, Raghavendran K. Influence of scan duration on pulmonary capillary hemorrhage induced by diagnostic ultrasound. *Ultrasound Med Biol* 2016; 42:1942–1950.

37. Nightingale KR, Church CC, Harris G, et al. Conditionally increased acoustic pressures in nonfetal diagnostic ultrasound examinations without contrast agents: a preliminary assessment. *J Ultrasound Med* 2015; 34:1–41.

38. Patterson B, Miller DL. Observation of acoustic fountain generation by diagnostic ultrasound shear wave elastography. *J Acoust Soc Am* 2018; 144:1670.